Multivariate, Multi-step, and Spatiotemporal Traffic Prediction for NextG Network Slicing under SLA Constraints

Evren Tuna[1,2] and Alkan Soysal[2,3]

[1]Department of Research & Development, ULAK Communications Inc., Ankara, Turkey

[2]Department of Electrical and Electronics Engineering, Bahcesehir University, Istanbul, Turkey

[3]Department of Electrical and Computer Engineering, Virginia Tech, Blacksburg, VA 24061

Abstract

This study presents a spatiotemporal traffic prediction approach for NextG mobile networks, ensuring the service-level agreements (SLAs) of each network slice. Our approach is multivariate, multi-step, and spatiotemporal. Leveraging 20 radio access network (RAN) features, peak traffic hour data, and mobility-based clustering, we propose a parametric SLA-based loss function to guarantee an SLA violation rate. We focus on single-cell, multi-cell, and slice-based prediction approaches and present a detailed comparative analysis of their performances, strengths, and limitations.

First, we address the application of single-cell and multi-cell training architectures. While single-cell training offers individual cell-level prediction, multi-cell training involves training a model using traffic from multiple cells from the same or different base stations. We show that the single-cell approach outperforms the multi-cell approach and results in test loss improvements of 11.4% and 38.1% compared to baseline SLA-based and MAE-based models, respectively.

Next, we explore slice-based traffic prediction. We present single-slice and multi-slice methods for slice-based downlink traffic volume prediction, arguing that multi-slice prediction offers a more accurate forecast. The slice-based model we introduce offers substantial test loss improvements of 28.2%, 36.4%, and 55.6% compared to our cell-based model, the baseline SLA-based model, and the baseline MAE-based model, respectively.

I. INTRODUCTION

The integration of key enablers, such as network slicing, private networks, and edge computing, tailored to specific services, has escalated the complexity of Next Generation (NextG) networks. Intelligent network management based on Machine Learning (ML) can address this complexity, enhancing the robustness, predictiveness, autonomy, and reliability of NextG cellular networks [1]–[3]. For instance, the Open Radio Access Network (RAN) paradigm employs near-real-time (10-1000 ms) and non-real-time (greater than 1 s) RAN Intelligent Controllers (RIC) for network management and control [4]. A network traffic forecast application at the non-real-time RIC can support applications at both the near-real-time RIC, such as network slicing, scheduling, mobility management, and radio resource management, and at the non-real-time RIC, like energy efficiency management.

Predicting network traffic in mobile networks necessitates analysis of substantial, highly dynamic past data, representing a complex, multi-dimensional problem. A comprehensive understanding of this problem from both data and communications perspectives is pivotal for implementing a practical solution in Open RAN. Notable dimensions in a NextG traffic prediction problem include temporal effects, spatial granularity, spatial clustering, feature selection, problem-specific optimization objectives, prediction horizon, and the transferability of the trained model to the operator's entire system.

Traditionally, temporal effects in time-series problems were addressed by variations of Autoregressive Integrated Moving Average (ARIMA) models [5]. For instance, [6] divided time series mobile traffic volume data into regular and random components. The regular component was predicted using ARIMA, resulting in a 30% error, whereas the random component was deemed unpredictable. Recently, ML methods have been applied to traffic volume prediction, yielding significantly better results than ARIMA models. Some ML-based works considered only temporal effects without spatial analysis where Long Short Term Memory (LSTM)-based Recurrent Neural Network (RNN) models outperformed statistical models like ARIMA [7]–[10]. These temporal-only analyses primarily focused on single time-series data from a single cell or aggregated data from multiple cells.

While prior works do not differentiate between spatial granularity and spatial clustering, it is

essential to understand the distinct impacts of both dimensions. When working with multiple time-series data from multiple cells, most prior works employ a grid-based spatial granularity, dividing the entire service area into smaller grids [11]–[16]. Traffic data from cells within the same grid are aggregated and treated as a single time series. This technique possibly results in lower prediction errors due to data smoothing but hinders mapping predicted data back to individual cells for cell-level intelligent control. The majority of grid-based approaches use Convolutional Neural Network (CNN)-based models to leverage spatial dependencies, drawing from CNN structures used in video processing applications. The matrix-format inputs represent the aggregated traffic of base stations in corresponding square grid areas. However, a persistent issue with grid-based spatial precision is its limited generalizability to a provider's entire service area. Despite these challenges, the grid-based approach has been gaining traction [17]–[27] leading to increasingly complex models that are likely overfitting and challenging to implement at the non-real-time RIC level.

In contrast to grid-level spatial granularity, other works have examined base station level [28]–[35] and cell level [36]–[39] spatial granularity. References [32], [33] use CNN at the base station level by rearranging base stations into a matrix structure. Conversely, [34]–[37] propose using graph convolutional networks (GCNs) instead. Here, the base stations or the cells are the graph nodes, and edges represent some interaction between cells. GCN implementation is challenging due to the need for pre-existing knowledge of all cell adjacency matrices, which should remain static over time. As a result, GCN may not be feasible for large-scale wireless systems [27].

The same works can also be classified according to their spatial clustering approach. Clustering is beneficial when data points (grids, base stations, cells) in the cluster interact. In proximity-based clustering, data points in close proximity are processed together [12]–[15], [17]–[24], [28]–[30], [37]. However, proximity does not necessarily indicate an interaction between cells [35]. In similarity-based clustering, data points exhibiting a certain similarity measure are processed together. Multiple similarity measures are considered in the literature, including correlation, k-shape, dynamic time warping, and spectral decomposition. Similarity does not necessarily indicate an interaction between cells, either. Alternatively, data volume at a neighboring cell might affect the data volume at the intended cell if there is handover between the cells. In

mobility-based clustering, handover data is used to cluster data points [35], [36], [38], [39]. While [35], [36] use handover data to calculate edge values in a GCN and suffer from GCN's shortcomings, our previous work [38], [39] can be dynamically applied to an entire network. Building upon [38], [39], we expand the scope of the research in this paper to incorporate multi-cell and slice-based approaches.

The majority of previous works utilize standard loss functions such as MAE, MSE, and their variants to minimize prediction errors. These symmetrical loss functions treat SLA violations and overprovisioning the same, resulting in nearly identical SLA violation and overprovisioning rates. However, operators prefer overprovisioning to SLA violations due to stringent SLA obligations, especially for slice-based network traffic. Since it is crucial to choose problem-specific optimization objectives, we propose a Service-Level Agreements (SLA) violation-based loss function for the traffic prediction problem in NextG network slicing. Traditional loss functions, such as MSE and MAE, are unsuitable for mobile operators who must maximize resource utilization while avoiding any SLA violations on network slices. Despite its importance, literature is limited in applications of SLA-based loss functions [32], [38], [39].

Our approach in this study is multivariate, multi-step, spatiotemporal, and SLA-driven. We investigate the effect of 20 different RAN features on predicting future values of downlink traffic volume. We devise additional feature sets based on peak traffic hours and extract the spatiotemporal effect of high mobility using incoming and outgoing handover relationships between cells. We perform multi-step prediction up to 24 hours ahead and propose a parametric SLA-based loss function to guarantee the SLA violation rate. We propose single-cell and multi-cell training architectures and assess their performance results. We predict slice-based traffic using a multi-slice architecture within a cell and calculate the total traffic at the cell level, achieving a lower SLA-based loss.

II. Dataset and Additional Features

This section presents the dataset and methodology used in this study, which primarily focuses on predicting the downlink traffic volume in a live RAN that serves a densely populated urban area with high user mobility. The dataset encompasses 30 base stations, corresponding to 135 cells, due to the presence of multiple sectors and carriers within each base station (see Fig. 1).
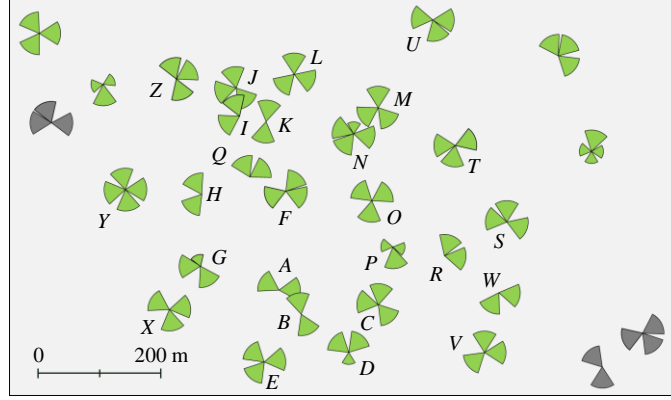
Fig. 1. Location of cells in our dataset.
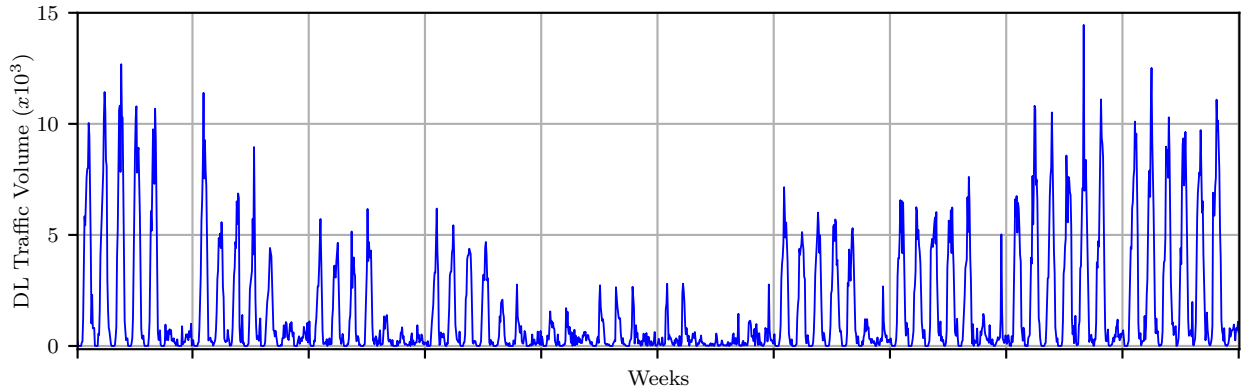
Fig. 2. Total downlink traffic volume of cell A_2 for a 10-week period.

For this study, letters denote base stations, and numbers denote the cells within a given base station. For instance, A_1 represents the first cell of base station A, while BS_n describes a generic cell within a generic base station.

The dataset comprises hourly measurements for each cell, encompassing both total and slice-based traffic metrics collected over a period of 52 weeks. Fig. 2 displays the hourly downlink traffic volume graph for a typical cell, A_2, located in a crowded city square. This cell experiences a heavy traffic load, with unexpected spikes during peak hours of the day. Besides daily fluctuations, the traffic volume is notably higher on weekdays than on weekends in some weeks. Moreover, the weekly average traffic volume changes week by week. These various dynamic behaviors make traffic prediction exceptionally challenging for such cells. We note that data aggregated at the base station or grid level granularity is significantly smoother due to the averaging of dynamic effects. The smoother the time series data, the better the prediction performance. Nevertheless, we choose to work with cell-level data, as it is essential for intelligent

(a) Voice slice.

(b) Data slice.

(c) FWA slice.
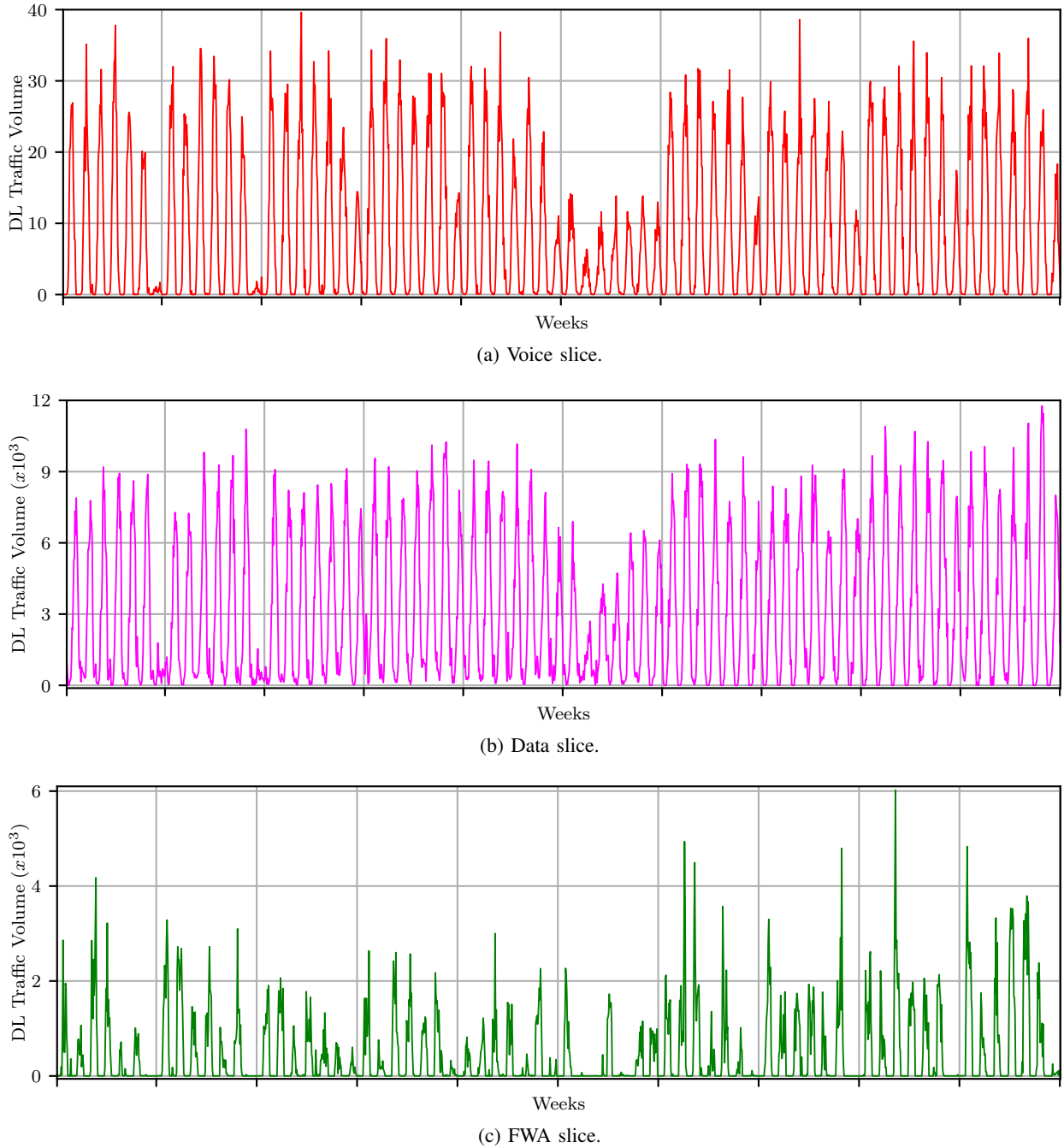
Fig. 3. Slice-based downlink traffic volume of cell A_2 for a 10-week period.

cell-level network control.

Slice-based measurements, available for a duration of 36 weeks, include traffic data for three distinct services: voice, data, and Fixed Wireless Access (FWA) for each cell. Fig. 3 illustrates the downlink traffic volume of each slice of cell A_2. The downlink traffic volume levels vary among each slice. Additionally, the voice and data slices display a more regular time series structure, while the FWA slice exhibits an irregular time series structure. These differences underscore the

TABLE I
RAN FEATURES

Label	Name
F0	Downlink Traffic Volume
F-RAN1	Avg. Num. of Active Users in downlink
F-RAN2	Avg. Num. of Active Users in uplink
F-RAN3	Num. of Avg. Simultaneous RRC Connected Users
F-RAN4	Downlink PRB Utilisation
F-RAN5	Uplink Traffic Volume
F-RAN6	Uplink PRB Utilisation
F-RAN7	Num. of RRC Attempts
F-RAN8	Num. of S1 Signalling Establishment Attempt
F-RAN9	Num. of Initial E-RABs Attempted to Setup
F-RAN10	RACH Setup Succ. Rate
F-RAN11	Downlink PDCP Cell Thr.
F-RAN12	Downlink PDCP User Thr.
F-RAN13	Uplink PDCP Cell Thr.
F-RAN14	Uplink PDCP User Thr.
F-RAN15	Avg. Uplink RSSI Weight PUCCH
F-RAN16	Avg. Uplink RSRP PUSCH
F-RAN17	Avg. Uplink RSRP PUCCH
F-RAN18	Avg. RACH Timing Advance
F-RAN19	Avg. CQI

importance of monitoring slice-based traffic.

Table I outlines the collected features of mobile network traffic with their respective measurement family names [40], [41]. The dataset includes 20 RAN features, with the total downlink traffic volume (labeled F0) being the output feature to be predicted.

An objective of our research is to enhance the performance of our model by incorporating additional input features beyond the downlink traffic volume. Initially, we examine the correlation between the downlink traffic volume and the other monitored features in the RAN. We anticipate that incorporating highly correlated features into the input dataset will positively impact the model's performance. We also introduce an additional feature set named *Peak Hours Feature*, which emphasizes specific time periods during the day. Lastly, we propose the *Mobility Clustering* method to address the spatiotemporal effect, which factors in the incoming and outgoing handover relationships. Below, we elaborate on the methods we use to extract these features.

A. RAN Features

We consider 20 different RAN features, whose labels are provided in Table I. We compute the Pearson correlation coefficient between the downlink traffic volume feature (F0) and the other features to identify the most correlated features. Fig. 4 illustrates the correlation heatmap for cell A_2.
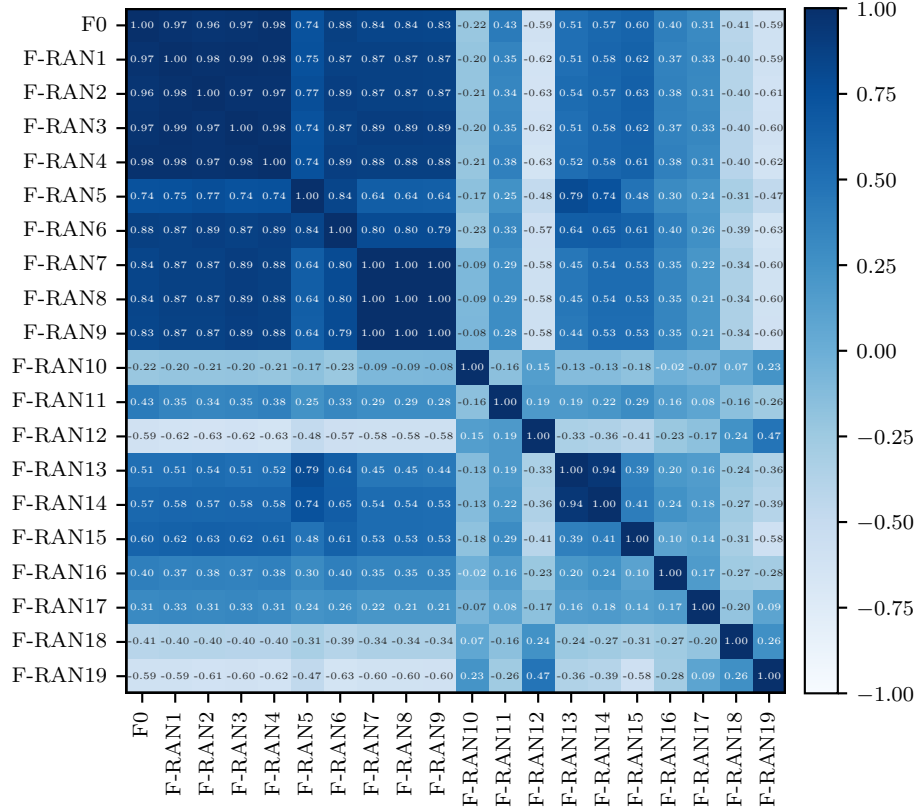
Fig. 4. Correlation heatmap of RAN features for cell A_2.

We establish a correlation threshold of 0.90 and examine the heatmap of various cells to determine the features that can be incorporated into the input dataset. In the total traffic dataset, we include features F-RAN1, F-RAN2, F-RAN3, and F-RAN4, in addition to the F0 feature. Conversely, for the slice-based traffic dataset, only F-RAN1 and F-RAN2 are included along with the F0 feature since F-RAN3 and F-RAN4 measurements are unavailable per slice. We denote the multivariate model that is based on RAN features as "mvLSTM-RAN".

B. Peak Hours

Our observations show that the F0 feature follows a 24-hour cycle for all cells, with intervals of low and high demand for traffic volume. In addition, F0 values are generally higher on weekdays and lower on weekends in densely populated urban areas. To capture these patterns, we introduce two additional Boolean feature vectors.

The first feature vector, "days of the week," distinguishes between weekdays and weekends in the input dataset. The second feature vector, "peak hours of the day," labels the hours that
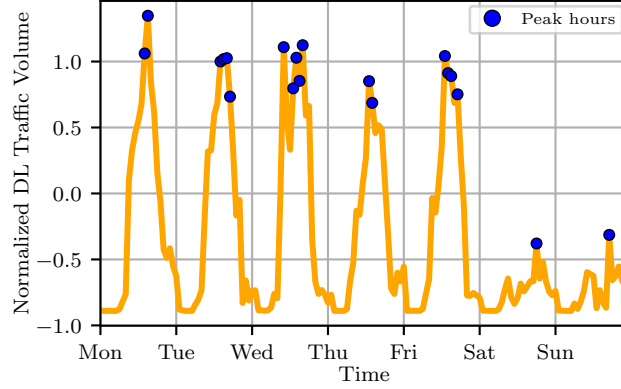
Fig. 5. The labels for the peak hours of the day in cell A_2.

have traffic volumes above 70% of the peak value. This differentiation helps distinguish peak hours from non-peak hours. Fig. 5 showcases the labeling of the peak hours of the day for cell A_2, marked with circles.

We refer to this multivariate model as "mvLSTM-peak", which integrates the "days of the week" and "peak hours of the day" vectors in addition to the F0 feature. It is important to note that these additional features are derived from the statistics of F0 and do not necessitate further RAN measurements.

C. Mobility Clustering

In densely populated areas with highly mobile users, the traffic volume demand experiences dynamic changes as users transition between cells. To better understand, let us concentrate on the coverage area of a highly dynamic cell, F_4, which exhibits significant handovers. Fig. 6 showcases our examination of the handover relationships of cell F_4, denoted in green. The arrows in Fig. 6—represented by red dashed, blue dashed dot, and purple dot lines—indicate the incoming, outgoing, and bidirectional handover relations of the cell.

Multiple strategies can be used to leverage the interaction between cells. The first approach is proximity clustering, where the features of all cells in the region help predict the traffic volume of the target cell, F_4. When we include all cells within 200 meters of the target cell, the prediction encompasses all cells in base stations $A, F, G, H, I, J, K, L, M, N, O, P$, and Q, denoted in gray. When we include cells whose coverage area intersects with the target cell, the prediction involves all cells in base stations K, L, N, O, and Q. In both instances, the proximity
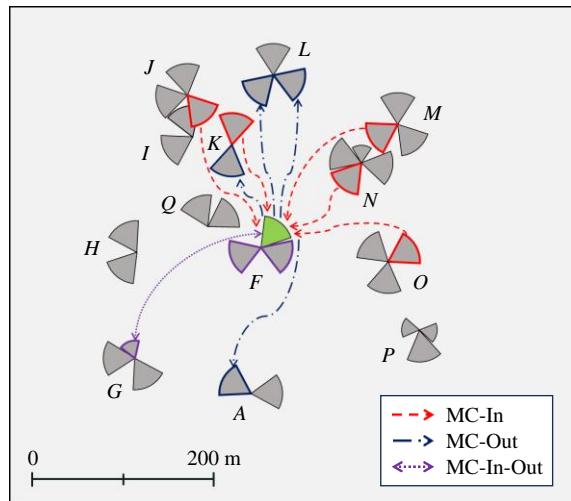
Fig. 6. Mobility clustering for cell F_4.

TABLE II
THE RATES OF INCOMING AND OUTGOING HANDOVERS FOR CELL F_4

Incoming		Outgoing	
Cells	**Rate %**	**Cells**	**Rate %**
N_2	18.34	F_1	32.44
F_3	17.72	N_2	17.83
F_2	9.84	F_3	7.18
M_3	7.49	M_3	6.75
F_1	5.51	G_3	4.38
F_{12}	4.88	F_{12}	4.35
G_3	4.68	O_5	3.36
J_1	4.32	J_1	3.34
O_5	4.23	L_5	2.28

clustering approach includes cells with no handover relationship to the target cell and excludes cells with a handover relationship. We assert that the handover relationship is the only means by which the traffic demand in one cell impacts the traffic demand in another cell. Therefore, we conclude that selecting cells in the cluster based solely on proximity and/or intersection of coverage does not improve prediction performance, underscoring the limitations of the grid structure of CNN-based approaches.

We propose the mobility clustering method to take advantage of the interaction between cells with handover relations. The cluster in this method only includes cells that maintain a handover relationship with the target cell F_4. Table II lists the neighboring cells that have incoming and outgoing handover relations with F_4. With mobility clustering, we expand the input dataset by incorporating two feature vectors. We construct these vectors by calculating the weighted averages of the downlink traffic volumes of the neighboring cells—one vector for

the incoming and the other for the outgoing handover relationship. We refer to this multivariate model as "mvLSTM-handover", which includes these two additional feature vectors derived through mobility clustering.

III. Neural Network Model with Parametric Loss Function

Our primary objective is to prevent SLA violations by developing a machine learning-based prediction method that considers multiple RAN features, unexpected traffic spikes during peak hours, and handovers between cells. To achieve this, we employ a multivariate LSTM architecture. While more complex models are available, we choose LSTM for several reasons: first, these more complex models cater to a grid-based approach that does not align with our focus on individual cells; second, the lengthy inference time of these complex models is impractical for the near-real-time RIC; third, our emphasis lies in mobility clustering, multivariate features, and an SLA-based loss function. This approach serves to strike a balance between computational feasibility and predictive accuracy, ensuring optimal network performance and resource allocation.

We introduce four multivariate LSTM models for predicting traffic volume in the RAN. The first model, mvLSTM-RAN, integrates additional RAN features. The second model, mvLSTM-peak, concentrates on the peak hours of the day and days of the week. The third model, mvLSTM-handover, includes the weighted averages of downlink traffic volumes of cells within the mobility cluster. Lastly, the mvLSTM-all model integrates all three multivariate models. Fig. 7 illustrates the total traffic input dataset structure of different LSTM models. We refer to the incoming and outgoing feature vectors acquired through the mobility clustering (MC) method as MC-In and MC-Out, respectively. For example, F0-MC-In signifies the vector obtained by weighted averaging the F0 vectors of the cells with incoming handover relationships to the relevant cell. It is worth noting that the mvLSTM-RAN model for slice-based traffic incorporates the F0, F-RAN1, and F-RAN2 features only.

To benchmark the performance of our multivariate model, we employ the univariate LSTM model as a reference. In the univariate model, the input comprises an array of the downlink traffic volume from the past 24 hours, and the output is the subsequent instance of the downlink
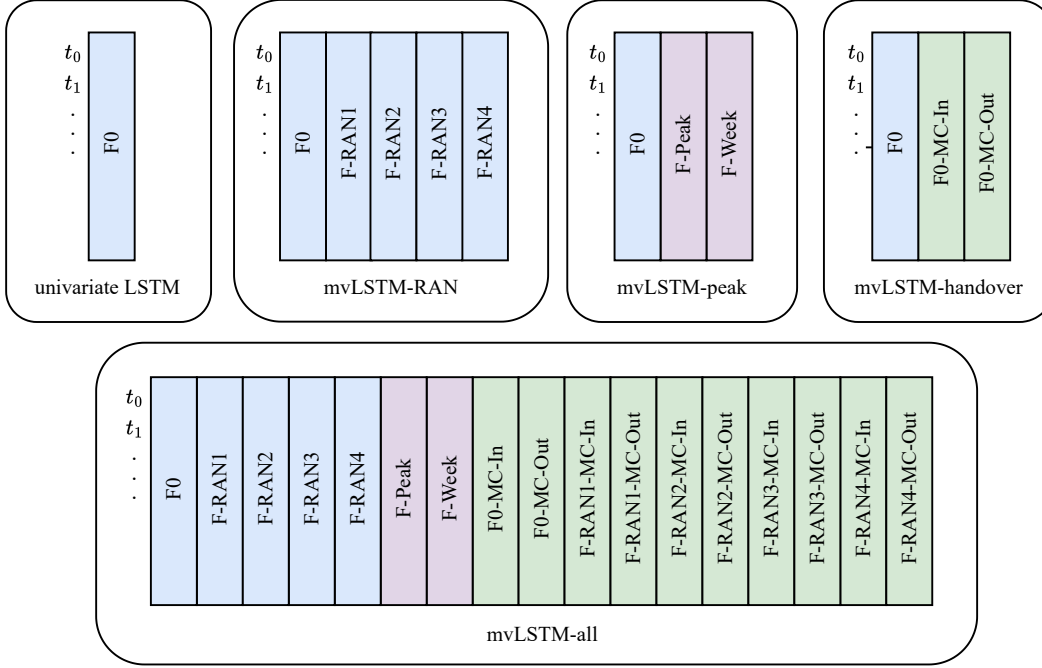
Fig. 7. The input datasets of total traffic for different LSTM models.

traffic volume. Conversely, in the multivariate models, the input consists of a list of arrays, each containing the past 24 hours of a specific feature.

We utilize the K-fold cross-validation technique to accommodate changing traffic levels and trends while training the model. We split the total traffic dataset into training, validation, and test sets with durations of 40 weeks, 8 weeks, and 4 weeks, respectively. We use 6 folds, subdividing the 48-week dataset into 8-week segments. Conversely, we split the slice-based dataset into training, validation, and test sets with durations of 24 weeks, 8 weeks, and 4 weeks, respectively. We use 4 folds, breaking up the 32-week dataset into 8-week segments. Each execution yields different training and validation sets by shifting the training dataset by 8 weeks. We normalize the feature sets using the mean and standard deviation values calculated from the training set.

After preprocessing the data, we focus on the model's loss function. Standard loss functions such as MAE and MSE present two significant disadvantages: first, they impose identical penalties for both SLA violations and overprovisioning; second, they cannot be parameterized with an SLA violation rate. Consequently, we introduce a parametric SLA-based loss function that overcomes both disadvantages of standard loss functions.

Let us denote y_n and $\mathbf{x}_n$ as the target value and input features of a prediction problem,

respectively, where n is the index of the elements in the dataset. Furthermore, let $f(\cdot)$ symbolize the input-output relationship of the DNN, determined by the network weights. We can express the predicted value as $\hat{y}_n(w) = f(\mathbf{x}_n, w)$, where w represents a loss function parameter. The training process seeks to minimize the average of a loss function, $\mathcal{L}(\cdot, w)$, to determine the DNN weights by using

$$\min_f \frac{1}{N_{\text{train}}} \sum_{n=1}^{N_{\text{train}}} \mathcal{L}\left(f(\mathbf{x}_n, w) - y_n, w\right). \tag{1}$$

Let us denote the prediction error as $e_n(w) = \hat{y}_n(w) - y_n$. During test time, an SLA violation occurs when the prediction error is negative, $e_n(w) < 0$, and overprovisioning takes place when the prediction error is positive, $e_n(w) > 0$. We define the SLA violation rate as the percentage of instances when an SLA is violated

$$r(w) = \frac{1}{N_{\text{test}}} \sum_{n=1}^{N_{\text{test}}} \mathbb{1}\left(-e_n(w)\right), \tag{2}$$

where N_{test} represents the number of elements in the test set, and $\mathbb{1}(\cdot)$ serves as the indicator function. It is crucial to understand that the SLA violation rate is not synonymous with the uptime or the outage rate. When traffic demand is underprovisioned (i.e., an SLA violation occurs), the customer continues to receive service but at a slightly diminished rate. Operators commonly utilize SLA violation rates of 1%, 3%, 5%, and 10%.

We define the overprovisioning volume as the average positive prediction error

$$v(w) = \frac{1}{\sum_{t=1}^{N_{\text{test}}} \mathbb{1}\left(e_n(w)\right)} \sum_{t=1}^{N_{\text{test}}} e_n(w) \mathbb{1}\left(e_n(w)\right). \tag{3}$$

After testing various parametric loss functions, we opt for the weighted Mean Absolute Error (wMAE) as the parametric loss function, which we define as

$$\mathcal{L}_{\text{wMAE}}(\hat{x} - x, w) = \begin{cases} w|\hat{x} - x|, & e \leq 0 \\ \hat{x} - x, & e > 0 \end{cases}. \tag{4}$$

Our goal is to minimize the SLA-based wMAE loss and overprovisioning volume while respecting a constraint on the SLA violation rate by choosing an appropriate w. We explore two different SLA violation rate scenarios, 3% and 5%, and conduct a line search to determine the
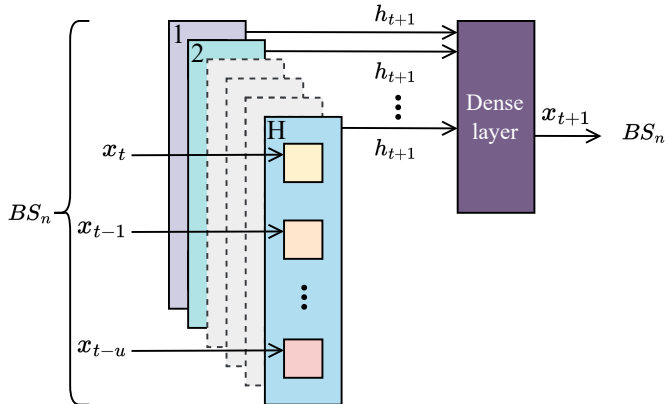
Fig. 8. Single-cell architecture, where an LSTM layer with window size u and H hidden units is followed by a dense layer.

optimal weights, denoted as $w_{3\%}$, and $w_{5\%}$.

IV. SINGLE-CELL PREDICTION

In this section, "single-cell" refers to training a model using the data from a single cell. Fig. 8 illustrates the single-cell architecture. The input features from a cell first undergo processing in the LSTM layer, where H and u represent the number of hidden units and window size, respectively. The output of the LSTM layer then moves into a dense layer, which produces F0 predictions for the cell in question. However, since a network might comprise thousands of cells, managing a separate model for each can become challenging and costly. We address this critical trade-off in subsequent sections. This section presents the single-step and multi-step prediction performance evaluation of the single-cell training architecture using the total traffic dataset.

A. Single-step Prediction

This subsection focuses on the effectiveness of our multivariate LSTM models in a single-step prediction scenario, where only the next time instance is predicted. We assess the performance of cell-based traffic volume predictions for typical base stations A and D under 3% and 5% SLA conditions. Specifically, we consider cells A_1, A_2, A_3, D_1, D_2, D_3, D_4, D_5, and D_6, all of which have different coverage areas.

Before delving into the performance of our proposed LSTM models, it is essential to understand why univariate models using traditional loss functions are inadequate for our specific

TABLE III

THE COMPARISON FOR THE SINGLE-STEP PREDICTION PERFORMANCE IN CELL A_2

Models	SLA-based loss	SLA%
ARIMA	5.51	83.60
MSE-based LSTM	0.83	42.66
LogCosh-based LSTM	0.67	31.55
Huber-based LSTM	0.66	30.56
MAE-based LSTM	0.63	29.56
Univariate LSTM	0.44	≤ 5
mvLSTM-RAN	0.43	≤ 5
mvLSTM-peak	0.44	≤ 5
mvLSTM-handover	0.39	≤ 5
mvLSTM-all	0.39	≤ 5

problem. Table III presents the SLA-based loss values and corresponding SLA violation percentages of traditional models and our proposed models using a 5% SLA violation constraint. Among the univariate LSTM models using traditional built-in loss functions, the most effective MAE-based LSTM incurs 43.2% higher SLA-based loss than the univariate LSTM model. More importantly, our proposed models maintain a given SLA violation rate. These points highlight the importance of our proposed models for the network traffic prediction problem.

Actual and predicted downlink traffic volumes appear in Fig. 9 for MAE-based univariate LSTM and mvLSTM-peak models. Although the predicted traffic curve in Fig. 9(a) seems to follow the actual traffic more closely than the predicted traffic curve in Fig. 9(b), error bars in Fig. 9(c) show significant SLA violations for MAE-based LSTM. In contrast, Fig. 9(d) presents very few SLA violations. MAE-based LSTM models generally result in SLA violations about half the time and lag behind actual traffic during peak hours. For SLA-based LSTM models, it is possible to adjust the level of SLA violations by tuning the weight parameter.

Table IV displays the cell-based test loss results for the A_1, A_2, and A_3 cells. SLA-based loss values for cell A_1 are much higher suggesting that traffic in A_1 is more dynamic. We observe that different models perform better for different cells. A change in the SLA violation rate also changes the best-performing model for A_2. When a lower SLA is targeted, using peak hours features proves more beneficial. These results underscore the limitations of a one-size-fits-all model for predicting multiple cells. Furthermore, they highlight the need for determining which additional features are most beneficial for individual cell traffic prediction.

Fig. 10 illustrates the predicted traffic curves of all models for cell A_2 under a stringent 3% SLA violation rate. Due to the strict SLA violation rate, nearly all models exhibit no negative

(a) Predicted traffic for the MAE-based LSTM model

(b) Predicted traffic for the mvLSTM-peak model

(c) Error bars for the MAE-based LSTM model

(d) Error bars for the mvLSTM-peak model
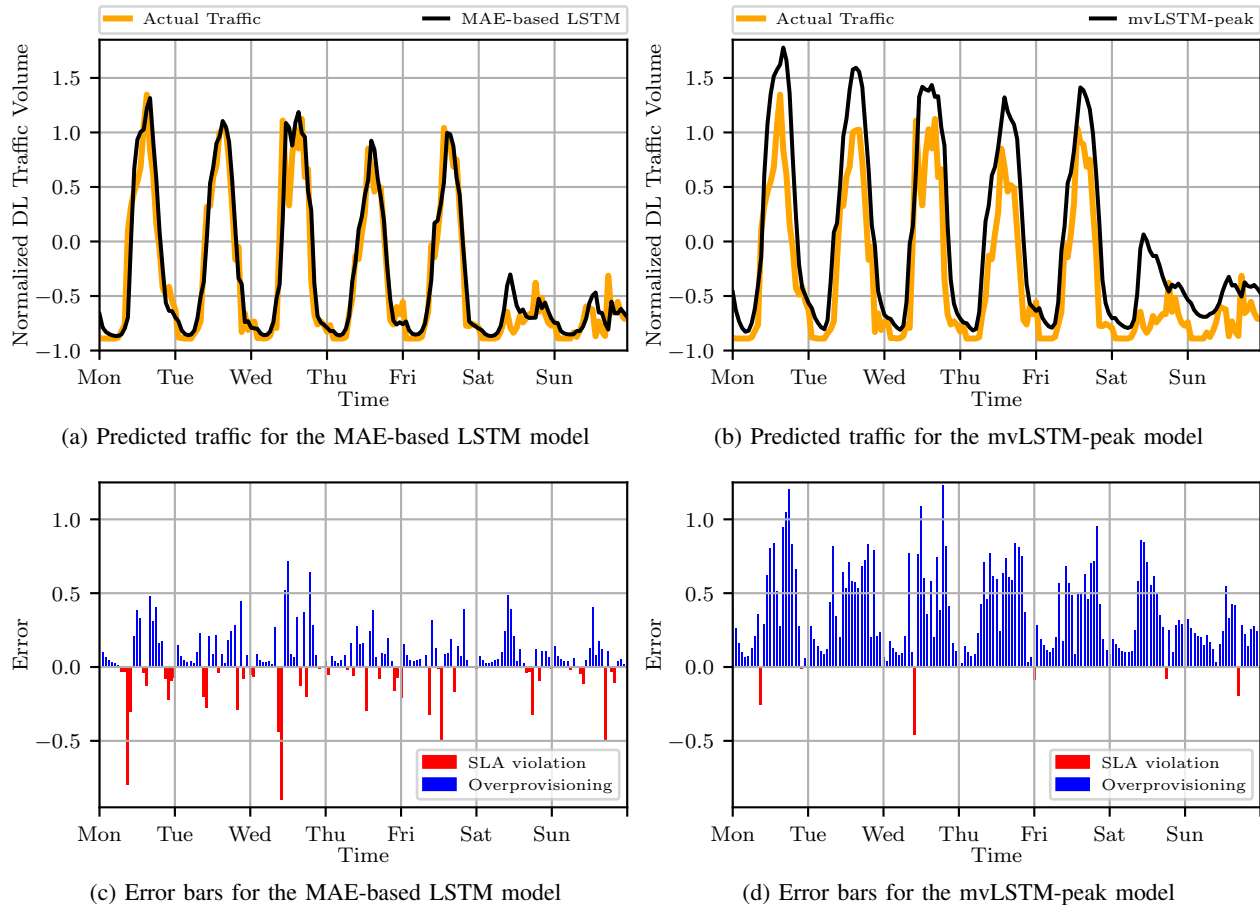
Fig. 9. Actual traffic, predicted traffic, and error values for cell A_2. Red lines are SLA violations.

TABLE IV
SLA-BASED LOSS VALUES FOR SINGLE-STEP PREDICTION OF BASE STATION A

Models	A_1		A_2		A_3	
	3%	**5%**	**3%**	**5%**	**3%**	**5%**
univariate LSTM	1.88	1.56	0.50	0.44	0.53	0.38
mvLSTM-RAN	**1.20**	**1.09**	0.49	0.43	0.64	0.48
mvLSTM-peak	1.43	1.23	**0.44**	0.44	0.49	0.39
mvLSTM-handover	1.70	1.17	**0.44**	**0.39**	0.63	0.52
mvLSTM-all	1.31	1.11	0.45	**0.39**	**0.47**	**0.38**

errors. Nonetheless, the mvLSTM-peak model proves superior in this context, yielding the lowest SLA-based loss and overprovisioning.

Next, to validate our findings from base station A, we explore another typical base station. Table V illustrates the cell-based performance results for cells D_1 through D_6. For base station D, we again observe that different models perform better for different cells. Using the same model for all cells in the system is not optimal, given that cells from different regions exhibit entirely different trends. We conclude that operators should consider cell-based prediction performance
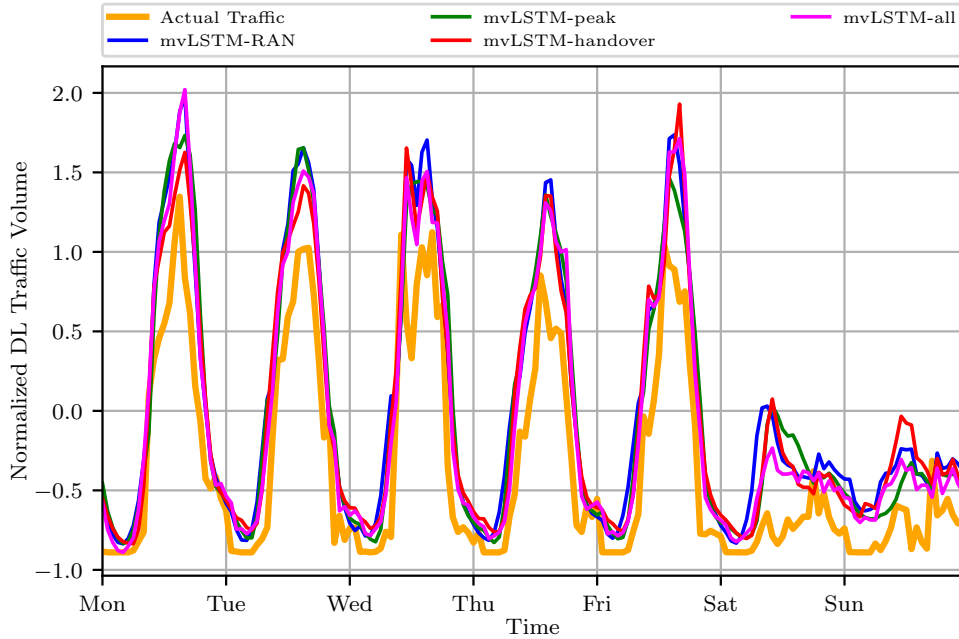
Fig. 10. Actual and predicted values for cell A_2 under 3% SLA violation rate.

TABLE V
SLA-BASED LOSS VALUES FOR SINGLE-STEP PREDICTION OF BASE STATION D

Models	D_1		D_2		D_3		D_4		D_5		D_6	
	3%	**5%**	**3%**	**5%**	**3%**	**5%**	**3%**	**5%**	**3%**	**5%**	**3%**	**5%**
univariate LSTM	0.61	0.53	0.79	0.78	0.78	0.70	1.52	1.40	0.45	0.39	0.75	0.66
mvLSTM-RAN	0.56	0.52	0.72	0.64	0.86	0.70	1.35	1.34	0.40	0.32	0.70	0.65
mvLSTM-peak	**0.51**	**0.48**	0.70	0.64	0.75	0.69	1.42	1.35	0.40	0.34	**0.67**	**0.63**
mvLSTM-handover	0.60	0.54	0.73	0.71	0.84	0.72	**1.34**	**1.28**	0.39	0.32	0.73	0.72
mvLSTM-all	0.54	0.51	**0.66**	**0.59**	**0.75**	**0.68**	1.36	1.40	**0.36**	**0.29**	0.68	0.66

when selecting a suitable prediction model for traffic volume prediction. As we have seen from the results in this subsection, even if different cells operate in the same base station, each has different coverage area characteristics and data patterns.

Another observation is that a model's SLA-based loss decreases as the SLA percentage increases. The weight for a 3% SLA is higher than for a 5% SLA, causing the loss function to penalize SLA violation cases more severely under the 3% SLA condition. Consequently, the model avoids violating the SLA more often, leading to increased test loss due to frequent overestimating of actual values.

TABLE VI
SLA-BASED LOSS VALUES FOR MULTI-STEP PREDICTION OF CELLS A_2 AND D_1 UNDER 5% SLA

Models	1-step		2-step		4-step		8-step		24-step	
	A_2	D_1	A_2	D_1	A_2	D_1	A_2	D_1	A_2	D_1
univariate LSTM	0.44	0.53	0.61	0.65	0.70	0.77	0.87	0.82	0.91	0.95
mvLSTM-RAN	0.43	0.52	0.49	0.60	0.56	0.62	0.77	0.79	1.00	1.08
mvLSTM-peak	0.44	**0.48**	0.76	0.66	**0.50**	0.60	**0.65**	**0.69**	**0.84**	**0.89**
mvLSTM-handover	**0.39**	0.54	**0.46**	**0.57**	0.57	0.63	0.89	0.83	1.07	0.91
mvLSTM-all	**0.39**	0.51	0.50	**0.57**	0.52	**0.58**	0.70	0.74	0.87	0.98

(a) Tue

(b) Thu
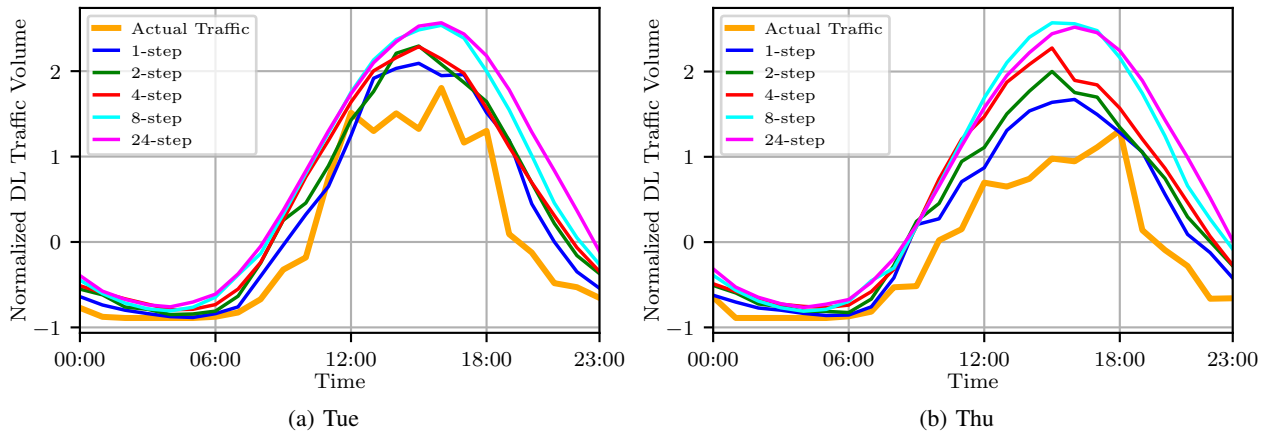
Fig. 11. Multi-step prediction using the mvLSTM-handover model for cell A_2.

B. Multi-step Prediction

In this subsection, we evaluate the effectiveness of our multivariate LSTM models in a multi-step prediction scenario. This section examines how much performance is affected by using multi-step prediction at the cell level. Specifically, we perform 1-hour, 2-hour, 4-hour, 8-hour, and 24-hour ahead predictions for cells A_2 and D_1. In a multi-step prediction scenario, previously predicted values serve as valid past values for subsequent predictions. Therefore, the accuracy of the initial prediction is crucial in determining the performance of the subsequent predictions.

Table VI shows SLA-based loss values of multi-step prediction for cells A_2 and D_1. For the mvLSTM-handover model, the SLA-based loss for the 2-hour ahead prediction is 17.9% higher than that of the 1-hour ahead prediction. As the number of steps in multi-step prediction increases, all models tend to overprovision more (higher loss values) during periods of rising and falling traffic demand. Furthermore, as the number of steps increases, the mvLSTM-peak model begins to outperform the mvLSTM-handover model. Fig. 11 displays the delay in model predictions as the number of steps increases.

As the number of steps increases in multi-step prediction, models are more likely to experience SLA violations and overprovisioning, which can reduce performance. On the other hand, using multi-step prediction can provide computational advantages as long as the degradation in performance is tolerable. Multi-step prediction can be used in regions with more stable traffic demand changes.

V. MULTI-CELL PREDICTION

This section discusses the multi-cell training architecture for network traffic prediction. Multi-cell training employs a single model with a multi-input multi-output structure, which takes traffic from multiple cells belonging to either the same base station (single-BS) or different base stations (multi-BS) as input. As explained in Section IV, single-cell training can become cumbersome when the network contains numerous cells. However, the training time increases in multi-cell training due to having a much larger dataset size and model complexity. Most existing literature adopts the multi-BS approach. However, this section demonstrates that the performance of the multi-BS approach falls short of the single-cell approach.

The single-BS approach involves training a unified model architecture using traffic from all cells operated by a single base station. It's important to clarify that we do not aggregate cell-based traffic in this approach; instead, we predict the traffic of each cell separately. The scenario depicted in Fig. 12 represents a single-BS architecture when the cells shown belong to the same base station.

On the other hand, multi-BS refers to training a larger model architecture using traffic from cells operating across multiple base stations. As with single-BS, no data aggregation is performed in the multi-BS approach, and we predict the traffic of each cell separately. The configuration shown in Fig. 12 constitutes a multi-BS architecture when the cells indicated belong to different base stations.

We initially feed the features for each cell into an LSTM layer. We then concatenate the outputs of the LSTM layers. Finally, the concatenated outputs feed into separate dense layers to produce F0 predictions for each cell. Applying mobility-based clustering in these approaches is still possible since the handover information serves as an additional feature of a given cell.
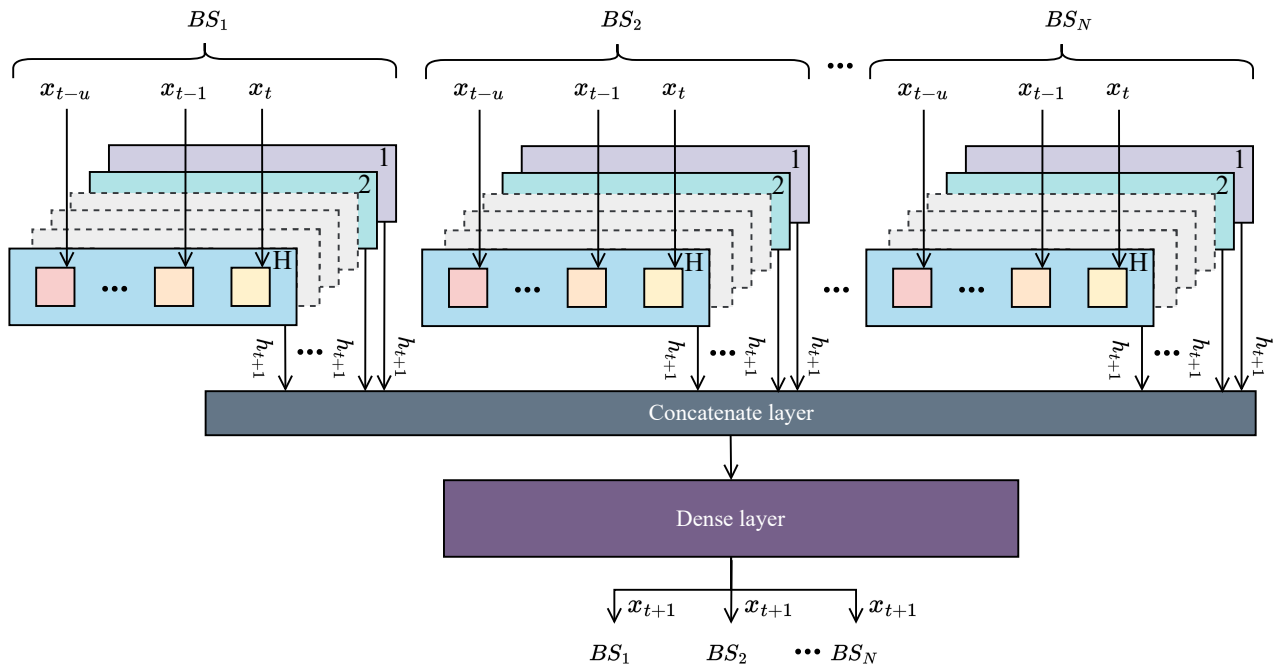
Fig. 12. Multi-cell architecture.

TABLE VII
SLA-BASED LOSS VALUES FOR SINGLE-CELL, SINGLE-BS AND MULTI-BS PREDICTION OF CELL A_2

Models	Single-cell	Single-BS	Multi-BS
univariate LSTM	0.44	0.44	**0.47**
mvLSTM-RAN	0.43	0.40	**0.47**
mvLSTM-peak	0.44	0.44	0.49
mvLSTM-handover	**0.39**	0.38	**0.47**
mvLSTM-all	**0.39**	**0.37**	0.49

Table VII exhibits the SLA-based loss values of single-cell, single-BS, and multi-BS predictions for cell A_2. The single-cell model considers the features of cell A_2 and generates that cell's prediction. Single-BS takes the features of the A_1, A_2, and A_3 cells from base station A and provides predictions for all cells within A. In contrast, multi-BS takes in the features of all 135 cells in our dataset and outputs the predictions for all cells within this network. In Table VII, we only report the results of cell A_2. The mvLSTM-all model outperforms the rest, showing a 11.4% and 15.9% reduction in test loss for single-cell and single-BS prediction, respectively, compared to the univariate LSTM model. For multi-BS prediction, the convergence of test loss values across different models suggests that the effects of model-specific multivariate features are less pronounced. Notably, the performance degradation observed during the transition from
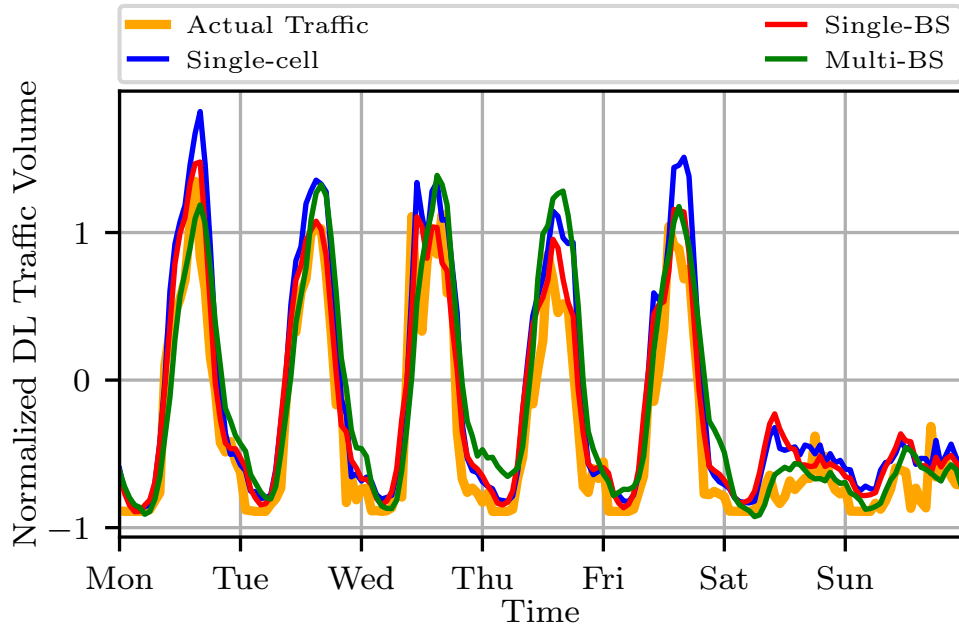
Fig. 13. Single-cell, single-BS and multi-BS prediction using the mvLSTM-all model for cell A_2.

single-cell to multi-BS, especially in the mvLSTM-all and mvLSTM-handover models, stresses the crucial role of handover effects for cell A_2. We can infer that complex and large models struggle to capture cell-specific information.

Fig. 13 shows that both single-cell and single-BS prediction models tend to overprovision slightly more during peak traffic demand hours throughout the week compared to multi-BS predictions. This tendency is advantageous in avoiding SLA violations. Furthermore, the single-cell prediction curve is more adept at tracking traffic peaks than the other models. In contrast, the multi-BS prediction curve exhibits a smoother pattern, which unfavorably impacts its ability to prevent SLA violations.

VI. Slice-based Traffic Prediction

In Sections IV and V, we employed methods to predict the *total* downlink traffic volume. In this section, however, we broaden our approach to forecasting the downlink traffic volume for various services provided by network slices created within cells. Different services offered through network slices possess distinct traffic patterns and dynamics. These variations can often be overlooked when assessing total traffic volume. Therefore, to achieve slice-based traffic prediction, it is crucial to treat the traffic data of each service separately.

Our dataset includes three distinct services: voice, data, and FWA, each of which can function as a slice. Voice services have evolved into Voice over LTE (VoLTE) and Voice over 5G (Vo5G), offering high-quality voice calls coupled with video conferencing and multimedia messaging. With the advent of 5G, data services are set to reach unparalleled speed, capacity, and responsiveness, propelling investments in network infrastructure optimization. Additionally, FWA provides a flexible and cost-effective alternative to wired broadband connections, using wireless technology to deliver high-speed internet access to fixed locations without needing physical cables or fiber optics. FWA proves particularly valuable in challenging areas and is perfect for residential, business, and remote locations requiring reliable broadband connectivity.

This section presents single-slice and multi-slice methods for slice-based downlink traffic volume prediction in a single-cell scenario. The single-slice method trains a model using the dataset specific to a network slice within a cell. Conversely, the multi-slice method trains a model using the dataset comprising all slices within the same cell, similar to the single-BS approach in Section V.

Table VIII illustrates the single-slice and multi-slice prediction performance results for cell A_2. Initially, we observe that the mvLSTM-peak and mvLSTM-all models perform best in the voice slice. Secondly, the mvLSTM-peak model exhibits the lowest SLA-based loss in the data slice in both scenarios. Particularly in the single-slice scenario, the gap in SLA-based loss between the mvLSTM-peak model and the univariate LSTM model reaches 25.5%. The peak hours feature benefits voice and data slices due to their more regular time series structure. However, the FWA slice registers the highest test loss for the univariate LSTM compared to other slices, suggesting that using univariate features is inadequate to capture fluctuations in FWA service demand. The mvLSTM-all model, which performs best, yields an SLA-based loss 31.8% lower than the univariate LSTM in single-slice prediction. Employing multivariate feature sets reduces the loss for all slices. Consequently, considering the demanding task of managing specific models for each slice, the multi-slice prediction method generally results in lower test loss than a single-slice prediction, making it the preferred approach.

Fig. 14 displays the actual and predicted traffic of single-slice and multi-slice prediction using the mvLSTM-all model for cell A_2. For the voice slice, the prediction values of the single-

TABLE VIII
SLA-BASED LOSS VALUES FOR SINGLE-SLICE AND MULTI-SLICE PREDICTION OF CELL A_2

Models	Voice		Data		FWA	
	Single-slice	Multi-slice	Single-slice	Multi-slice	Single-slice	Multi-slice
univariate LSTM	0.40	0.34	0.51	0.37	0.88	0.61
mvLSTM-RAN	0.38	0.32	0.43	0.38	0.64	0.61
mvLSTM-peak	**0.34**	0.33	**0.38**	**0.34**	0.72	0.61
mvLSTM-handover	0.40	0.36	0.59	0.44	0.67	0.62
mvLSTM-all	0.36	**0.31**	0.45	0.40	**0.60**	**0.55**
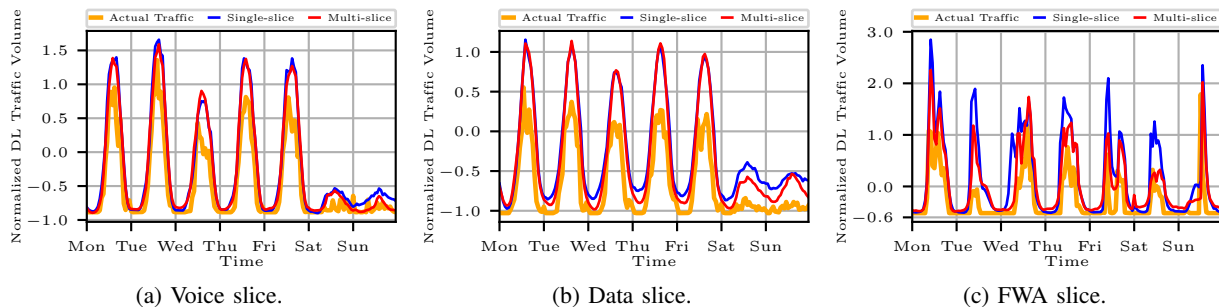
Fig. 14. Actual traffic and predicted traffic of single-slice and multi-slice prediction using the mvLSTM-all model for cell A_2.

slice approach are generally higher than those of the multi-slice approach during peak hours and weekends, resulting in higher SLA-based loss for the single-slice method. The single-slice approach leads to more overprovisioning during non-peak hours and weekends in the data slice. The single-slice approach shows extremely high prediction values during peak traffic hours in the FWA slice. Additionally, on Wednesday, it causes significant overprovisioning as it accurately anticipates the surge in traffic demand a few hours in advance.

In addition to resulting in lower test loss and overprovisioning, another advantage of slice-based prediction is the ability to assign different SLA constraints to different services, which is the norm in NextG mobile networks. Table IX presents a comparison of test loss results at the slice level under different SLA conditions for total downlink traffic volume of cell A_2, using the mvLSTM-all model. Here, we compare the average of all slices under various SLA conditions with the single-cell result at 5% SLA condition, as shown in Table IV. The comparison reveals that as we assign different SLA conditions to different slices, the performance of slice-based prediction surpasses that of the single-cell prediction. Let us consider the configuration where the SLA constraints of voice, data, and FWA slices are 5%, 10%, and 15%, respectively. Such a configuration prioritizes the voice slice, allowing for more SLA violations in the FWA

TABLE IX
SLA-BASED LOSS VALUES FOR MULTI-SLICE PREDICTION WITH SLICE SPECIFIC SLA CONSTRAINTS

SLA%	Voice	Data	FWA	Average	No slice
(1, 5, 10)	0.42	0.32	0.43	0.39	0.39
(3, 5, 10)	0.34	0.30	0.39	0.34	0.39
(5, 10, 15)	0.35	0.23	0.24	0.28	0.39

slice. Compared to the mvLSTM-model and univariate LSTM model results listed in Table IV, the slice-based prediction improvements in this configuration can rise to 28.2% and 36.4%, respectively.

VII. CONCLUSION

In this study, we have delved into the challenging problem of traffic prediction for NextG mobile networks, emphasizing the need for intelligent management and optimization of these complex systems. Our method incorporates 20 RAN features, additional features based on peak traffic hours, and a unique mobility-based clustering scheme to capture and utilize spatiotemporal effects. The devised parametric loss function is crucial in safeguarding the SLAs violation rate while reducing overprovisioning and ensuring reliable service delivery and resource utilization.

The paper thoroughly examined single-cell, multi-cell, and slice-based prediction approaches. Each approach brings unique strengths and challenges, shedding light on the intricacies of managing and predicting traffic in extensive mobile network environments. The exploration of slice-based traffic prediction is particularly relevant with the rise of network slicing in 5G networks. By focusing on the downlink traffic volume of various services offered within network slices, we pave the way for precise resource allocation and optimization.

Our comparative analysis highlights the performance and accuracy of the multi-slice prediction approach. This result signifies the potential of this method in effectively handling the diverse and dynamically changing traffic patterns within NextG networks. In addition, we find that using the same model for all cells in the network is not optimal, given that cells from different regions exhibit entirely different trends.

However, the scope for further research and improvement remains. As NextG networks evolve, the complexity and dynamism of traffic patterns will continue to increase, necessitating even more refined prediction techniques. Future research can explore transferring the single-cell approach

to an extensive network, collecting more mobility data, or developing an adaptive loss function to adjust to the changing SLA requirements.

REFERENCES

[1] R. Shafin, L. Liu, V. Chandrasekhar, H. Chen, J. Reed, and J. C. Zhang, "Artificial intelligence-enabled cellular networks: A critical path to beyond-5G and 6G," *IEEE Wireless Communications*, vol. 27, no. 2, pp. 212–217, Apr. 2020.

[2] C. Zhang, P. Patras, and H. Haddadi, "Deep learning in mobile and wireless networking: A survey," *IEEE Communications Surveys & Tutorials*, vol. 21, no. 3, pp. 2224–2287, 2019.

[3] M. Wang, Y. Cui, X. Wang, S. Xiao, and J. Jiang, "Machine learning for networking: Workflow, advances and opportunities," *IEEE Network*, vol. 32, no. 2, pp. 92–99, 2018.

[4] M. Polese, L. Bonati, S. D'Oro, S. Basagni, and T. Melodia, "Understanding o-ran: Architecture, interfaces, algorithms, security, and research challenges," *IEEE Communications Surveys & Tutorials*, vol. 25, no. 2, pp. 1376–1411, 2023.

[5] N. Bui, M. Cesana, S. A. Hosseini, Q. Liao, I. Malanchini, and J. Widmer, "A survey of anticipatory mobile networking: Context-based classification, prediction methodologies, and optimization techniques," *IEEE Communications Surveys Tutorials*, vol. 19, no. 3, pp. 1790–1821, 2017.

[6] F. Xu, Y. Lin, J. Huang, D. Wu, H. Shi, J. Song, and Y. Li, "Big data driven mobile traffic understanding and forecasting: A time series approach," *IEEE Transactions on Services Computing*, vol. 9, no. 5, pp. 796–805, 2016.

[7] H. D. Trinh, L. Giupponi, and P. Dini, "Mobile Traffic Prediction from Raw Data Using LSTM Networks," in *IEEE PIMRC*, Sep. 2018, pp. 1827–1832.

[8] C. Gutterman, E. Grinshpun, S. Sharma, and G. Zussman, "RAN Resource Usage Prediction for a 5G Slice Broker," in *ACM MobiHoc*, ser. Mobihoc '19. Association for Computing Machinery, Jul. 2019.

[9] W. Wang, C. Zhou, H. He, W. Wu, W. Zhuang, and X. Shen, "Cellular Traffic Load Prediction with LSTM and Gaussian Process Regression," in *IEEE ICC*, Jun. 2020.

[10] H. Chergui and C. Verikoukis, "Offline sla-constrained deep learning for 5g networks reliable and dynamic end-to-end slicing," *IEEE Journal on Selected Areas in Communications*, vol. 38, no. 2, pp. 350–360, 2020.

[11] J. Wang, J. Tang, Z. Xu, Y. Wang, G. Xue, X. Zhang, and D. Yang, "Spatiotemporal modeling and prediction in cellular networks: A big data enabled deep learning approach," in *IEEE INFOCOM*, 2017.

[12] C.-W. Huang, C.-T. Chiang, and Q. Li, "A study of deep learning networks on mobile traffic forecasting," in *International Symposium on Personal, Indoor, and Mobile Radio Communications (PIMRC)*, 2017, pp. 1–6.

[13] L. Chen, D. Yang, D. Zhang, C. Wang, J. Li, and T.-M.-T. Nguyen, "Deep mobile traffic forecast and complementary base station clustering for c-ran optimization," *Journal of Network and Computer Applications*, vol. 121, pp. 59–69, 2018.

[14] C. Zhang and P. Patras, "Long-term mobile traffic forecasting using deep spatio-temporal neural networks," in *ACM MobiHoc*, Jun. 2018.

[15] C. Zhang, H. Zhang, D. Yuan, and M. Zhang, "Citywide cellular traffic prediction based on densely connected convolutional neural networks," *IEEE Communications Letters*, vol. 22, no. 8, pp. 1656–1659, 2018.

[16] C. Zhang, H. Zhang, J. Qiao, D. Yuan, and M. Zhang, "Deep Transfer Learning for Intelligent Cellular Traffic Prediction Based on Cross-Domain Big Data," *IEEE Journal on Selected Areas in Communications*, vol. 37, no. 6, pp. 1389–1401, Jun. 2019.

[17] M. Li, Y. Wang, Z. Wang, and H. Zheng, "A deep learning method based on an attention mechanism for wireless network traffic prediction," *Ad Hoc Networks*, vol. 107, p. 102258, oct 2020.

[18] N. Zhao, Z. Ye, Y. Pei, Y.-C. Liang, and D. Niyato, "Spatial-Temporal Attention-Convolution Network for Citywide Cellular Traffic Prediction," *IEEE Communications Letters*, vol. 24, no. 11, pp. 2532–2536, Nov. 2020.

[19] W. Shen, H. Zhang, S. Guo, and C. Zhang, "Time-Wise Attention Aided Convolutional Neural Network for Data-Driven Cellular Traffic Prediction," *IEEE Wireless Communications Letters*, vol. 10, no. 8, pp. 1747–1751, Aug. 2021.

[20] Q. Liu, J. Li, and Z. Lu, "ST-Tran: Spatial-Temporal Transformer for Cellular Traffic Prediction," *IEEE Communications Letters*, vol. 25, no. 10, pp. 3325–3329, Oct. 2021.

[21] H. Wu, J. Wang, and C. Liu, "TAN: Temporal Attention Enhanced Network for Cellular Traffic Prediction," in *Proc. WCSP*, Nov. 2022.

[22] Z. Li, Y. Fu, P. Zhao, and C. Li, "A Dynamic Spatiotemporal Prediction Method for Urban Network Traffic," in *IEEE VTC2022 Fall*, Sep. 2022.

[23] Y. Hu, Y. Zhou, J. Song, L. Xu, and X. Zhou, "Citywide Mobile Traffic Forecasting Using Spatial-Temporal Downsampling Transformer Neural Networks," *IEEE Transactions on Network and Service Management*, vol. 20, no. 1, pp. 152–165, Mar. 2023.

[24] Z. Rao, Y. Xu, S. Pan, J. Guo, Y. Yan, and Z. Wang, "Cellular Traffic Prediction: A Deep Learning Method Considering Dynamic Nonlocal Spatial Correlation, Self-Attention, and Correlation of Spatiotemporal Feature Fusion," *IEEE Transactions on Network and Service Management*, vol. 20, no. 1, pp. 426–440, Mar. 2023.

[25] Z. Wang, J. Hu, G. Min, Z. Zhao, Z. Chang, and Z. Wang, "Spatial-Temporal Cellular Traffic Prediction for 5G and Beyond: A Graph Neural Networks-Based Approach," *IEEE Transactions on Industrial Informatics*, vol. 19, no. 4, pp. 5722–5731, Apr. 2023.

[26] Y. Yao, B. Gu, Z. Su, and M. Guizani, "MVSTGN: A Multi-View Spatial-Temporal Graph Network for Cellular Traffic Prediction," *IEEE Transactions on Mobile Computing*, vol. 22, no. 5, pp. 2837–2849, May 2023.

[27] A. Mehrabian, S. Bahrami, and V. W. Wong, "A dynamic bernstein graph recurrent networkfor wireless cellular traffic prediction for wireless cellular traffic prediction," in *IEEE ICC*, 2023.

[28] C. Qiu, Y. Zhang, Z. Feng, P. Zhang, and S. Cui, "Spatio-temporal wireless traffic prediction with recurrent neural network," *IEEE Wireless Communications Letters*, vol. 7, no. 4, pp. 554–557, 2018.

[29] J. Feng, X. Chen, R. Gao, M. Zeng, and Y. Li, "Deeptp: An end-to-end neural network for mobile cellular traffic prediction," *IEEE Network*, vol. 32, no. 6, pp. 108–115, 2018.

[30] Y. Gao, X. Wei, L. Zhou, and H. Lv, "A Deep Learning Framework with Spatial-Temporal Attention Mechanism for Cellular Traffic Prediction," in *IEEE Globecom Workshops*, Dec. 2019.

[31] X. Xing, Y. Lin, H. Gao, and Y. Lu, "Wireless Traffic Prediction with Series Fluctuation Pattern Clustering," in *IEEE ICC Workshops*, Jun. 2021.

[32] D. Bega, M. Gramaglia, M. Fiore, A. Banchs, and X. Costa-Pérez, "DeepCog: Optimizing Resource Provisioning in Network Slicing With AI-Based Capacity Forecasting," *IEEE Journal on Selected Areas in Communications*, vol. 38, no. 2, pp. 361–376, Feb. 2020.

[33] Z. Wang and V. W. Wong, "Cellular Traffic Prediction Using Deep Convolutional Neural Network with Attention Mechanism," in *IEEE ICC*, May 2022.

[34] X. Chen, G. Chuai, K. Zhang, and W. Gao, "Spatial-temporal Cellular Traffic Prediction: A Novel Method Based on Causality and Graph Attention Network," in *IEEE WCNC*, Mar. 2023.

[35] X. Wang, Z. Zhou, F. Xiao, K. Xing, Z. Yang, Y. Liu, and C. Peng, "Spatio-temporal analysis and prediction of cellular traffic in metropolis," *IEEE Transactions on Mobile Computing*, vol. 18, no. 9, pp. 2190–2202, 2019.

[36] S. Zhao, X. Jiang, G. Jacobson, R. Jana, W.-L. Hsu, R. Rustamov, M. Talasila, S. A. Aftab, Y. Chen, and C. Borcea, "Cellular network traffic prediction incorporating handover: A graph convolutional approach," in *IEEE SECON*, 2020.

[37] L. Fang, X. Cheng, H. Wang, and L. Yang, "Mobile demand forecasting via deep graph-sequence spatiotemporal modeling in cellular networks," *IEEE Internet of Things Journal*, vol. 5, no. 4, pp. 3091–3101, 2018.

[38] E. Tuna and A. Soysal, "Multivariate Spatio-temporal Cellular Traffic Prediction with Handover Based Clustering," in *CISS*, Mar. 2022.

[39] ——, "Multivariate and Multi-step Traffic Prediction for NextG Networks with SLA Violation Constraints," in *BalkanCom*, Jun. 2023.

[40] "Telecommunication management; Performance Management (PM); Performance measurements E-UTRAN," 3GPP, Technical Specification (TS) 32.425, 06 2021, version 17.1.0.

[41] "Telecommunication management; Performance Management (PM); Concept and requirements," 3GPP, Technical Specification (TS) 32.401, 04 2022, version 17.0.0.